

Importance of Tropospheric Correction to C-band InSAR Measurements: Application in the 2018 Palu Earthquake

Hidayat Panuntun

Geomatics Laboratory, Department of Earth Technology, Vocational College, Universitas Gadjah Mada, Indonesia

Leni Sophia Heliani

Department of Geodetic Engineering, Faculty of Engineering, Universitas Gadjah Mada, Indonesia

Wiwit Suryanto

Seismology Research Group, Geophysics, Universitas Gadjah Mada, Indonesia

Cecep Pratama

Department of Geodetic Engineering, Faculty of Engineering, Universitas Gadjah Mada, Indonesia

Received: 2021-10-17

Accepted: 2022-10-13

Keywords:

2018 Palu earthquake;
Postseismic deformation; InSAR,
Sentinel-1; Generic atmospheric
correction online service

Abstract Long-term InSAR-based observations are prone to atmospheric delay interference. The active-phase signals emitted and recorded back by sensors during imaging are easily disturbed by the electron content in the ionospheric layer and the water vapor content in the tropospheric layer. Given that the short wavelength of the C-band used by Sentinel-1 is more sensitive to tropospheric delay than to ionospheric delay, in this work, we utilized InSAR Sentinel-1 data to observe the postseismic deformation that occurred following the 2018 Palu earthquake and to evaluate the effect of tropospheric delay on the estimated interferogram time series. The cloud computation of Looking into Continent from Space with Synthetic Aperture Radar (LiCSAR) and LiCSBAS was used to generate interferograms and analyze the time series. Here the atmospheric delay was modeled by using Generic Atmospheric Correction Online Service (GACOS) and removed from the generated interferograms. Results showed that the annual velocity and cumulative line-of-sight (LOS) displacement were refined by correcting the atmospheric delay. Specifically, by applying GACOS, the standard deviation of the generated interferograms decreased by up to 76.6%. GNSS observations were utilized to verify the improvement due to the removal of tropospheric noise. We found that LOS displacement with GACOS correction better fitted the GNSS observation than LOS displacement without GACOS correction. Therefore, atmospheric correction plays an important role in long-term InSAR-based observations, especially in avoiding any bias in the interpretation of the estimated time series.

Correspondent email:

hidayat.panuntun@ugm.ac.id

©2022 by the authors. Licensee Indonesian Journal of Geography, Indonesia.
This article is an open access article distributed under the terms and conditions of the Creative Commons Attribution (CC BY NC) license <https://creativecommons.org/licenses/by-nc/4.0/>.

1. Introduction

InSAR observation has shown to be a valuable tool for identifying the deformation induced by a variety of geophysical phenomena, including tectonic (e.g., Panuntun, 2021; Qiu, Ji, Liu, & Liu, 2019) and volcanic activities (e.g., Albino, Biggs, Yu, & Li, 2020; Pepe et al., 2019). Continuous GNSS measurement is one of the most popular methods for monitoring surface deformation (X. He et al., 2017). It can provide data with excellent temporal resolution. However, continuous GNSS monitoring is time-consuming and only provides point-wise data (i.e., it has low spatial resolution). Hence, the capabilities of the InSAR technique in providing high-density observation over a large area distinctly highlight the advantages of InSAR measurement over GNSS especially under the condition of sparse GNSS measurement.

The accuracy of InSAR observations is highly affected by the noise that originates from atmospheric nuisance signals. The InSAR community regularly calls this effect atmospheric delay (Z. Li et al., 2019). Two kinds of atmospheric delay are widely known by geoscientists: (1) ionospheric delay, which originates from the interaction between the satellite signal and the free electron content in the ionospheric layer (e.g., H. Fattahi,

Simons, & Agram, 2017), and (2) tropospheric delay, which originates from the water vapor content in the tropospheric layer (e.g., Heresh Fattahi & Amelung, 2015). The presence of these disturbances can be very problematic because it can mask the actual surface displacement over long observation periods. For example, Heresh Fattahi and Amelung (2015) found that the annual tropospheric delay with the maximum amplitude of 10 cm could introduce biases of up to 24 cm into InSAR line-of-sight (LOS) displacement.

Previous studies have reported that the short wavelength of the C-band is less affected by the noise from the ionospheric layer than that from the tropospheric layer (e.g., Liang, Agram, Simons, & Fielding, 2019). Consequently, in Sentinel-1 SAR images, bias due to tropospheric delay is more prominent than that due to ionospheric delay. Previous works have revealed that at least two strategies for reducing the effect of tropospheric delay have been proposed: the internal correction method (e.g., Bekaert, Hooper, & Wright, 2015) and the external data-driven correction method (e.g., Z. W. Li et al., 2012; Mears, Wang, Smith, & Wentz, 2015; Yu, Li, Penna, & Crippa, 2018). Essentially, the internal correction method relies on the phased measurement without additional data from

external resources, whereas the external correction method uses an external dataset that includes data from the ground-based instrument, the space-based instrument, and weather.

An earthquake with a moment magnitude of 7.5 occurred on 28 September 2018. The U.S Geological Survey (USGS, 2018) reported that the earthquake epicenter is located at 0.256°S and 119.846°E with a depth of 20 km (Figure 1). The USGS further classified this earthquake as a strike–slip faulting event with dominant left-lateral motion. Previous studies (e.g., L. He et al., 2019; Song et al., 2019) reported that this earthquake ruptured two fault segments with a total length of approximately 250 km. Most previous works (e.g., Bacques et al., 2020; Fang et al., 2019; L. He et al., 2019; Socquet, Hollingsworth, Pathier, & Bouchon, 2019; Song et al., 2019) used InSAR to estimate the earthquake source model because GNSS observations in this area are relatively sparse. Generally, previously published coseismic slip models have similar conclusions for this event: (1) the coseismic slip mechanism is dominated by left-lateral strike–slip motion and (2) the mainshock had broken some segments along the Palu–Koro Fault with supershear velocity.

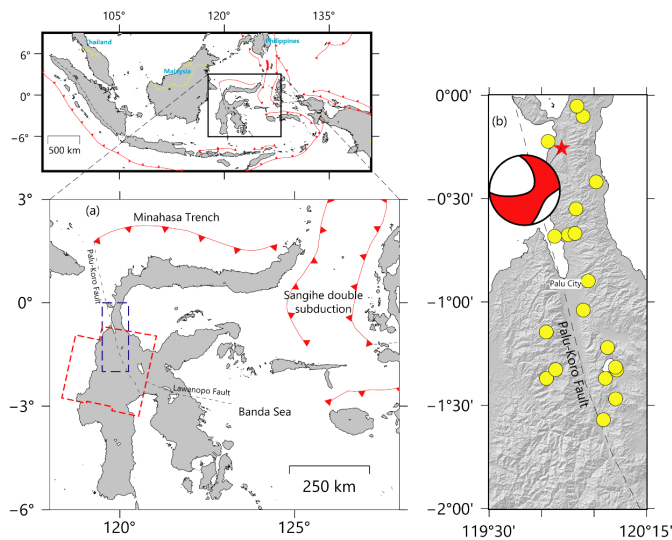


Figure 1. Tectonic setting around the 2018 Palu earthquake.

(a) Sulawesi Island. Red continuous lines represent the trench line around Sulawesi Island. Red dashed lines show the Looking into Continent from Space with Synthetic Aperture Radar frame used in this study. Black dashed lines denote the identified active fault in Sulawesi Island. (b) Epicenter of the 2018 Palu earthquake. Yellow circles represent aftershocks 1 year after the 2018 Palu Earthquake. Beach ball denotes the focal mechanism of the mainshock from USGS.

In contrast to coseismic study data, InSAR data have not been extensively used to investigate the postseismic deformation that occurred following the 2018 Palu earthquake. Utilizing InSAR data in postseismic deformation studies requires careful processing, including correction for tropospheric delay, because postseismic signals are considerably weaker than coseismic signals. Here, we use Sentinel-1 data to study postseismic deformation following the 2018 Palu earthquake.

Tropospheric correction provided by Generic Atmospheric Correction Online Service (GACOS) is used to remove noise signals due to tropospheric delay. GACOS is one of the most advanced external tropospheric correction methods (Yu et al., 2018). Instead, of simply relying on a single external dataset,

GACOS combines multiple datasets from weather and GNSS observations to create tropospheric correction maps for almost all over the world. Consequently, this method has become the preferred method used by previous studies to mitigate the effect of tropospheric noise (Albino et al., 2020; Kang et al., 2021; Watson, Elliott, & Walters, 2022). We then investigated the extent of improvements by applying the correction to InSAR data.

2. Methods

Data

Here, interferograms were created from Sentinel-1 data. The data were imaged by using the Sentinel-1 satellite system that is launched and operated by the European Space Agency. The Looking into Continent from Space with Synthetic Aperture Radar (LiCSAR) system, an autonomous cloud interferometric computing system, is used to alleviate the computational burden associated with creating interferograms from SLC images (Lazeký et al., 2020). In this study, we used one frame covering the broken segment of the Palu–Koro Fault with the observation period from October 2018 to February 2021 (see Figure 1a). The frame was generated by the LiCSAR system by using the Sentinel-1 data observed in Terrain Observation by Progressive Scans-Interferometric Wide mode from descending orbit path 134. The unwrapped interferograms were obtained by applying SNAPHU, whereas GACOS was used to model and remove the atmospheric noise error (Yu et al., 2018).

Notably, the naming format of LiCSAR system data is different from the original Sentinel-1 SLC data. Each frame has the pattern OOP-AAAAA-BBBBBB, where OOP is the relative orbit number, P is the orbital direction (i.e., A for ascending and D for descending), AAAAA is the colatitude identifier, andBBBBB is the number of contained bursts (Lazeký et al., 2020). The frame number used in this study is 134D_09191_141311. The selected frame had images acquired from descending track 134 and consisted of 583 interferograms derived from 125 acquisitions (see Figure 1a). The frame was cropped to the study's interest region to focus better on the observed postseismic deformation along the Palu–Koro Fault.

GACOS correction

GACOS was developed by (Yu et al., 2018) during his stay at Newcastle University. It is one of the options for atmospheric correction for InSAR observations that is available for wide use. Generally, this correction combines the global high-resolution weather model with the zenith tropospheric delay (ZTD) measurement of global network GPS stations. Specifically, the stratified and turbulent components were extracted from tropospheric delays by applying the iterative tropospheric decomposition model (Yu, Penna, & Li, 2017), thus generating a high-resolution ZTD map. GACOS has some notable features over other corrections. It has global coverage under near real-time and all-weather conditions. GACOS is an easy-to-use correction due to its free online services. Specifically, the user only needs to submit a request with their specific date of InSAR observation and boundary of the study area. The system will proceed with the submitted requests and generate the GACOS-ZTD product in tens of minutes.

InSAR time series: processing strategy

Processing multiple interferograms to create interferometric time series requires a powerful in-house processing computer machine, as well as a large amount of data storage resources.

In short, powerful resources are needed to estimate InSAR time series flawlessly. Thus, in this study, the generation of interferogram time series was estimated by using LiCSBAS to minimize the computational burden (Morishita *et al.*, 2020).

Interferogram time series are created in LiCSBAS in two phases (Figure 2): (1) unwrapped data stack preparation and (2) time series analysis. Five stages are required to complete stack preparation: (a) acquisition of LiCSAR products, (b) conversion of the file format, (c) removal of atmospheric noise with GACOS, (d) masking of areas with poor coherence, and (e) clipping to a specified interest area. Six stages are required to complete the time series analysis: (a) verifying the interferogram quality, (b) verifying the loop closure and detecting defective interferograms, (c) performing small baseline inversion calculation, (d) calculating the standard deviation of velocity, (e) masking, and (f) filtering time series.

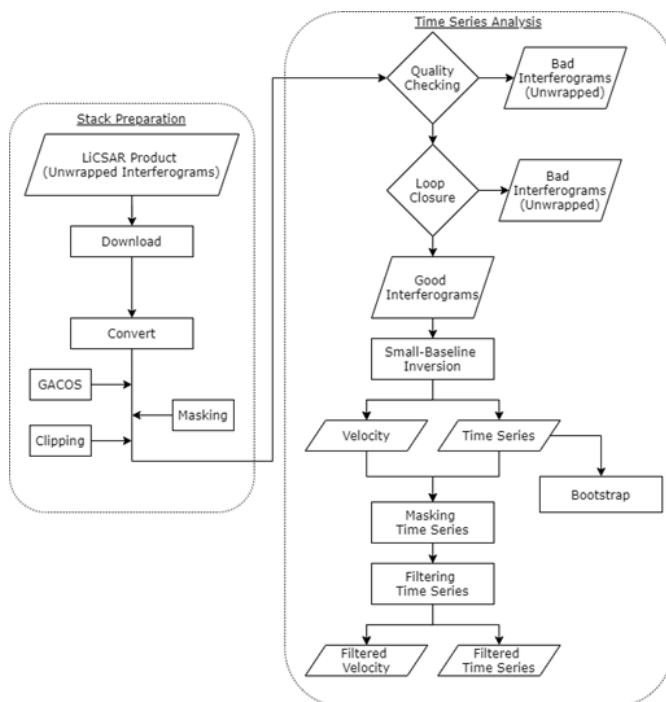


Figure 2. Work flow of LiCSBAS (modified from Morishita *et al.*, 2020).

In this study, the masked threshold value was set as ≤ 0.1 to minimize the effect of unwrapping errors. The temporal filter width was set as 0.2 years to capture tiny fluctuations in the estimated time series. Velocity was calculated by using the small baseline inversion technique (e.g., Bernardino, Fornaro, Lanari, & Sansosti, 2002). Notably, short spatial and temporal baselines may cause gaps during inversion. Gaps may also be caused by low coherence values and the lack of data observation. Thus, during inversion, the temporal constraint was imposed to eliminate gaps in the resulting time series. The other parameter settings of LiCSBAS were set as default.

3. Result and Discussion

The noise due to atmospheric delay may cause severe problems in detecting weak tectonic signals and smearing the observed ground displacement. Here, we show that by applying the GACOS model, the standard deviation of the interferograms is reduced to 76.6% (Figure 3). We then used GNSS observations to verify the improvement due to the removal of tropospheric noise. Specifically, we compared the cumulative postseismic displacement observed by three GNSS

receivers 325 days following the mainshock located near the Palu–Koro fault (Nijholt, Simons, Efendi, Sarsito, & Riva, 2021) with that observed by using the InSAR technique (before and after applying GACOS). Our results demonstrate that LOS displacement without GACOS correction tend to overestimate the observed displacement. Conversely, fitting to the GNSS observations is improved by applying GACOS (Figure 4).

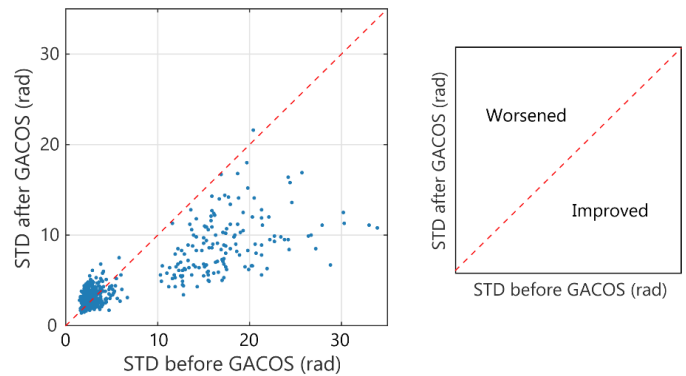


Figure 3. Scatter plot showing the improvement in standard deviation after GACOS correction. Black dots represent the generated interferograms. Black dots below the red dashed line indicate the improvement in an interferogram after GACOS application.

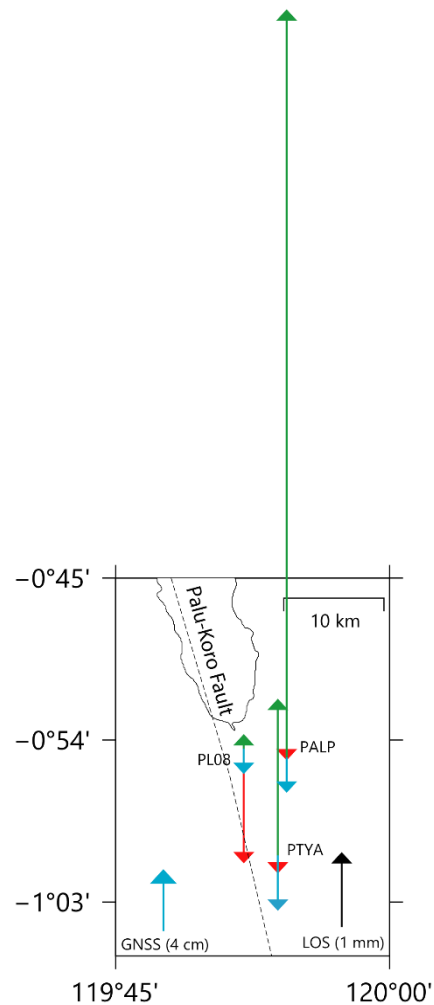


Figure 4. Comparison of the observed displacement at selected points. Blue, red, and green arrows represent the observed displacement from GNSS, LOS with GACOS, and LOS without GACOS. Note that GNSS and LOS observations have different scales.

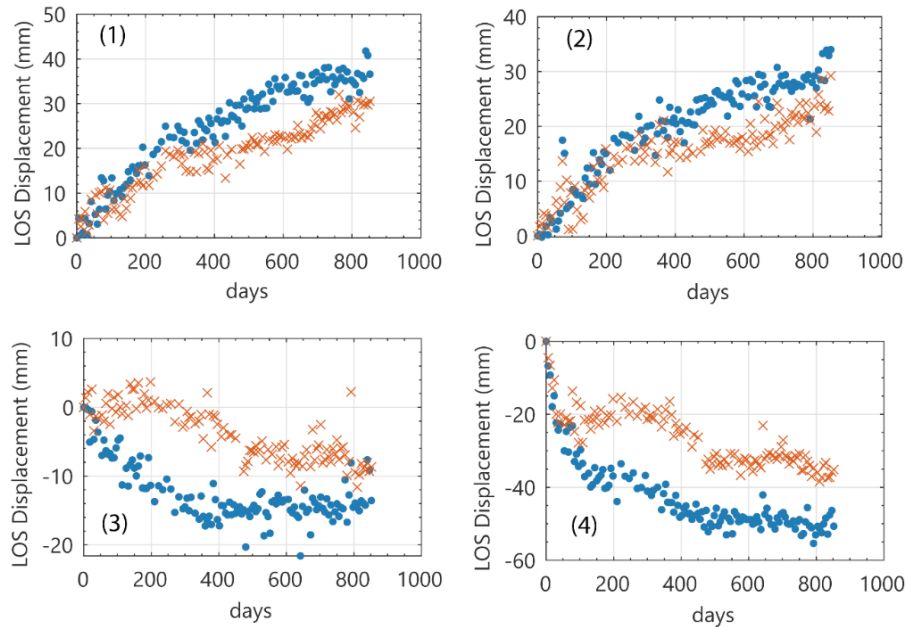


Figure 5. Comparison of the LOS time series at selected points (see the location of this selected point in Figure 7a). Blue dots represent the time series with GACOS. Brown crosses represent the time series without GACOS.

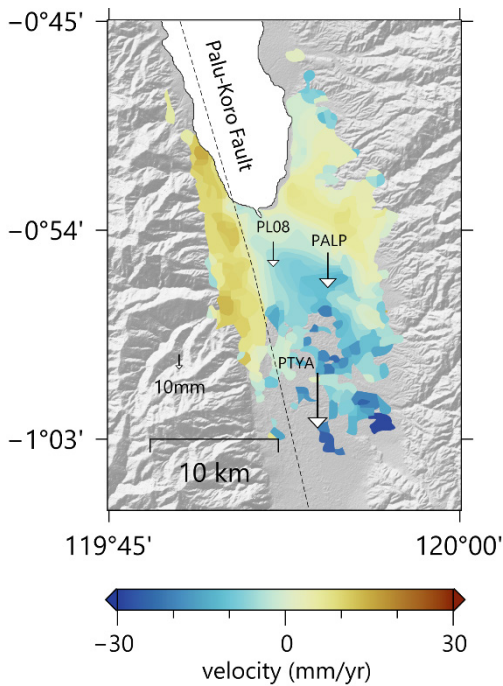


Figure 6. LOS vs GNSS vertical displacement. Black arrows represent the selected GNSS data of Nijholt et al. (2021). Positive and negative values indicate the movement toward (e.g., uplift) and away (e.g., subsidence) from the satellite sensor, respectively.

Figure 5 shows the comparison of the estimated time series with and without GACOS at a selected point. We notice that atmospheric delay tends to reduce the postseismic signal and underestimate the observed ground displacement. Additionally, the sudden pattern change is most likely due to the atmospheric artifact.

Postseismic deformation observed by satellite data helps us gain further insight into the kinematics and seismic potential of the active fault. Here, we find that Sentinel-1 data clearly illustrate the postseismic deformation that occurred following the 2018 Palu earthquake. Figure 6 shows the LOS velocity observed by InSAR data ~2.3 years after the 2018 Palu

earthquake. Significant uplift is located in the western side of the Palu–Koro Fault with the maximum rate of ~27 mm/year. By contrast, the eastern side of the Palu–Koro Fault is dominated by subsidence with the maximum rate of ~47 mm/year. The U–D component of the 3D position obtained from the selected GNSS observation has a similar trend as the LOS observation (see black arrows in Figure 6). Specifically, the postseismic deformation observed by GNSS (e.g., Nijholt et al., 2021; Pratama, Meilano, Sunarti, Haksama, & Sulistiyo, 2020) shows that this area is undergoing subsidence. Given that the subsidence motion detected by the LOS observation is consistent with that detected by the GNSS observation, we conclude that the estimated time series produced by LiCSBAS is valid.

Some previous studies (e.g., Hu, Bürgmann, Freymueller, Banerjee, & Wang, 2014; Panuntun, Miyazaki, Fukuda, & Orihara, 2018) used a specific fitting function to detect outliers in the estimated time series. Logarithmic and exponential decay functions are the most common functions that have been used to fit postseismic time series (Tobita, 2016). Here, we then use the following logarithmic function to fit the selected time series:

$$y = a \times \log\left(1 + \frac{t}{c}\right), \quad (1)$$

where t represents the observation date, and a and b denote the constant estimated by inverting the LOS displacement time series. The root mean square of the fitting residual has clearly improved after atmospheric correction is introduced (Figures 7b and 7c). This situation suggests that GACOS can help reduce the outliers in data observation. These results further suggest that GACOS plays an important role in postseismic time series generation.

Figure 8 shows the cumulative LOS displacement over ~2.3 years after the mainshock. The cumulative LOS uplift and subsidence reach ~55 and ~111 mm, respectively. The clear spatial pattern of the observed LOS displacement suggests that the postseismic deformation following the mainshock decayed rapidly. However, the short wavelength of the Sentinel-1 sensor cannot deeply penetrate vegetation. This inability thus leads to the loss of coherence. Consequently,

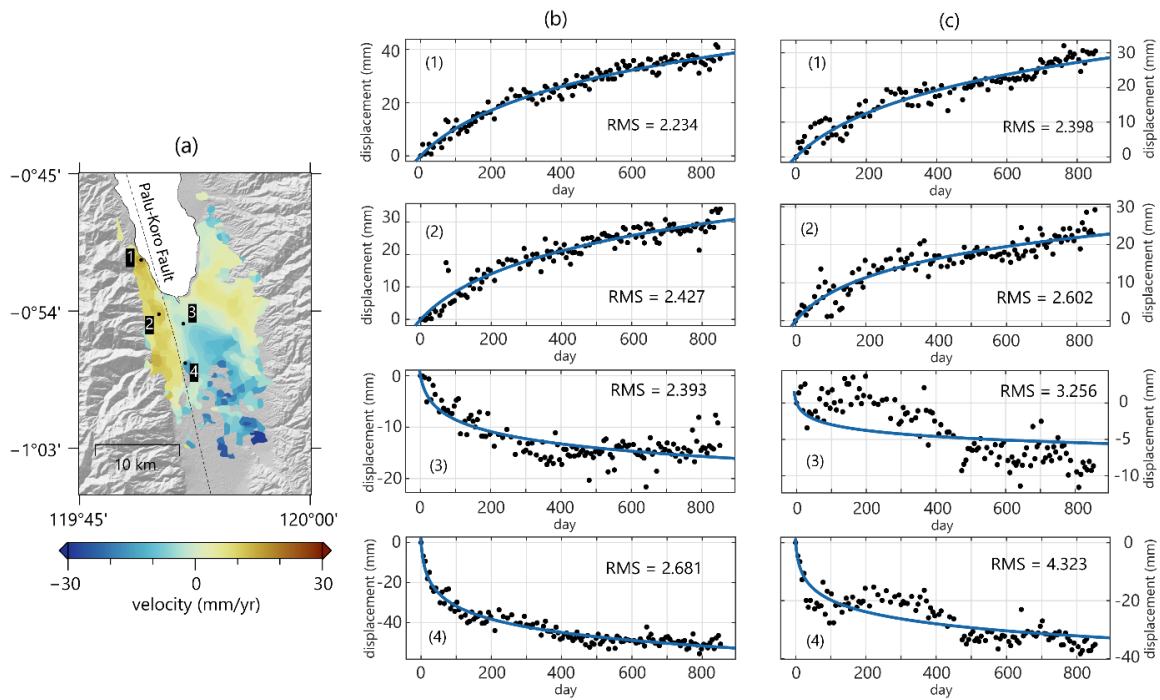


Figure 7. Example of the time series at selected locations. (a) LOS velocity rate map. Black dots with numbers indicate the location of the selected point (b) Time series and its logarithmic fitting function with GACOS and (c) without GACOS. Black dashed line represents the Palu–Koro Fault. Positive and negative values indicate the movement toward (e.g., uplift) and away (e.g., subsidence) from the satellite sensor, respectively.

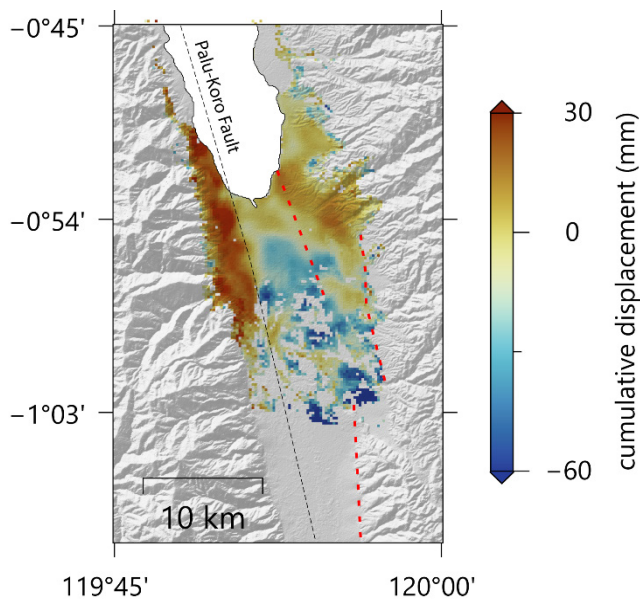


Figure 8. Cumulative LOS displacement over ~2.3 years following the mainshock. Black dashed line denotes the Palu–Koro Fault. Positive (red color) and negative (blue color) values indicate the movement toward (e.g., uplift) and away (e.g., subsidence) from the satellite sensor, respectively. Red dashed lines indicate the complex fault systems located in the eastern side of Palu City (Jaya, Nishikawa, & Jumadil, 2019).

the created interferogram only covers a relatively small area in and around Palu City. Previous studies (e.g., Fang *et al.*, 2019; Socquet *et al.*, 2019) observed the peak coseismic slip at the fault segment in this area.

Our results show that the region with significant subsidence is surrounded by uplift patterns in the western and eastern sides. In the western side, the subsidence pattern is clearly

cut by the Palu–Koro fault (see Figure 8). However, previous coseismic studies (e.g., Fang *et al.*, 2019; Socquet *et al.*, 2019; Song *et al.*, 2019) did not report any fault trace in the eastern side of Palu City. In other words, displacement discontinuity in this area is invisible during the rupture phase. However, a field survey by Jaya *et al.* (2019) found a trace of the cross-basin fault system. InSAR observation did not identify surface deformation during the coseismic period. This situation suggests that this fault system might be tectonically inactive before the mainshock. Additionally, given that this feature is observed after the mainshock, the increased uplift rate in this region might have been triggered by the 2018 earthquake.

4. Conclusion

Sentinel-1 images were used to investigate the postseismic deformation that occurred after the 2018 Palu earthquake. Interferogram generation and time series analysis were performed by using LiCSAR and LiCSBAS, respectively. GACOS was used to model and remove atmospheric artifacts from the generated interferograms. The extent of the improvements was then investigated by applying the correction to the InSAR data. The results showed that GACOS can help reduce the noise due to tropospheric delay. Specifically, by applying GACOS, the standard deviation of the formed interferograms decreased by up to 76.6%. GNSS observation was utilized to verify the improvement due to the removal of tropospheric noise. LOS displacement with GACOS correction had better fit to the GNSS observation than that without GACOS correction. The annual velocity and cumulative LOS displacement were refined by correcting the atmospheric delay. The maximum LOS uplift was ~55 mm, whereas the maximum LOS subsidence reached ~111 mm approximately 2.3 years after the 2018 Palu earthquake. The results of this work demonstrated that atmospheric correction plays an important role in postseismic time series generation.

Acknowledgments

Most of figures in this manuscript were generated by using GMT software (Wessel et al., 2019). This research was funded by Penelitian Dasar Unggulan Perguruan Tinggi 2021. We are thankful to the anonymous reviewer who provided constructive and critical comments and to Dr. Pramaditya Wicaksono for his editorship.

References

- Albino, F., Biggs, J., Yu, C., & Li, Z. (2020). Automated Methods for Detecting Volcanic Deformation Using Sentinel-1 InSAR Time Series Illustrated by the 2017–2018 Unrest at Agung, Indonesia. *Journal of Geophysical Research: Solid Earth*, *125*(2), e2019JB017908. doi:<https://doi.org/10.1029/2019JB017908>
- Bacques, G., de Michele, M., Foumelis, M., Raucoules, D., Lemoine, A., & Briole, P. (2020). Sentinel optical and SAR data highlights multi-segment faulting during the 2018 Palu-Sulawesi earthquake (Mw 7.5). *Scientific Reports*, *10*(1), 9103. doi:[10.1038/s41598-020-66032-7](https://doi.org/10.1038/s41598-020-66032-7)
- Bekaert, D. P. S., Hooper, A., & Wright, T. J. (2015). A spatially variable power law tropospheric correction technique for InSAR data. *Journal of Geophysical Research: Solid Earth*, *120*(2), 1345–1356. doi:<https://doi.org/10.1002/2014JB011558>
- Berardino, P., Fornaro, G., Lanari, R., & Sansosti, E. (2002). A new algorithm for surface deformation monitoring based on small baseline differential SAR interferograms. *IEEE Transactions on Geoscience and Remote Sensing*, *40*(11), 2375–2383. doi:[10.1109/TGRS.2002.803792](https://doi.org/10.1109/TGRS.2002.803792)
- Fang, J., Xu, C., Wen, Y., Wang, S., Xu, G., Zhao, Y., & Yi, L. (2019). The 2018 Mw 7.5 Palu Earthquake: A Supershear Rupture Event Constrained by InSAR and Broadband Regional Seismograms. *Remote Sensing*, *11*(11), 1330.
- Fattahi, H., & Amelung, F. (2015). InSAR bias and uncertainty due to the systematic and stochastic tropospheric delay. *Journal of Geophysical Research: Solid Earth*, *120*(12), 8758–8773. doi:<https://doi.org/10.1002/2015JB012419>
- Fattahi, H., Simons, M., & Agram, P. (2017). InSAR Time-Series Estimation of the Ionospheric Phase Delay: An Extension of the Split Range-Spectrum Technique. *IEEE Transactions on Geoscience and Remote Sensing*, *55*(10), 5984–5996. doi:[10.1109/TGRS.2017.2718566](https://doi.org/10.1109/TGRS.2017.2718566)
- He, L., Feng, G., Li, Z., Feng, Z., Gao, H., & Wu, X. (2019). Source parameters and slip distribution of the 2018 Mw 7.5 Palu, Indonesia earthquake estimated from space-based geodesy. *Tectonophysics*, *772*, 228216. doi:<https://doi.org/10.1016/j.tecto.2019.228216>
- He, X., Montillet, J.-P., Fernandes, R., Bos, M., Yu, K., Hua, X., & Jiang, W. (2017). Review of current GPS methodologies for producing accurate time series and their error sources. *Journal of Geodynamics*, *106*, 12–29. doi:<https://doi.org/10.1016/j.jog.2017.01.004>
- Hu, Y., Bürgmann, R., Freymueller, J. T., Banerjee, P., & Wang, K. (2014). Contributions of poroelastic rebound and a weak volcanic arc to the postseismic deformation of the 2011 Tohoku earthquake. *Earth, Planets and Space*, *66*(1), 106. doi:<https://doi.org/10.1186/1880-5981-66-106>
- Jaya, A., Nishikawa, O., & Jumadil, S. (2019). Distribution and morphology of the surface ruptures of the 2018 Donggala–Palu earthquake, Central Sulawesi, Indonesia. *Earth, Planets and Space*, *71*(1), 144. doi:[10.1186/s40623-019-1126-3](https://doi.org/10.1186/s40623-019-1126-3)
- Kang, Y., Lu, Z., Zhao, C., Xu, Y., Kim, J.-w., & Gallegos, A. J. (2021). InSAR monitoring of creeping landslides in mountainous regions: A case study in Eldorado National Forest, California. *Remote Sensing of Environment*, *258*, 112400. doi:<https://doi.org/10.1016/j.rse.2021.112400>
- Lazecský, M., Spaans, K., González, P. J., Maghsoudi, Y., Morishita, Y., Albino, F., Elliott, J., Greenall, N., Hatton, E., Hooper, A., Juncu, D., McDougall, A., Walters, R. J., Watson, C. S., Weiss, J. R., & Wright, T. J. (2020). LiCSAR: An Automatic InSAR Tool for Measuring and Monitoring Tectonic and Volcanic Activity. *Remote Sensing*, *12*(15). doi:[10.3390/rs12152430](https://doi.org/10.3390/rs12152430)
- Li, Z., Cao, Y., Wei, J., Duan, M., Wu, L., Hou, J., & Zhu, J. (2019). Time-series InSAR ground deformation monitoring: Atmospheric delay modeling and estimating. *Earth-Science Reviews*, *192*, 258–284. doi:<https://doi.org/10.1016/j.earscirev.2019.03.008>
- Li, Z. W., Xu, W. B., Feng, G. C., Hu, J., Wang, C. C., Ding, X. L., & Zhu, J. J. (2012). Correcting atmospheric effects on InSAR with MERIS water vapour data and elevation-dependent interpolation model. *Geophysical Journal International*, *189*(2), 898–910. doi:<https://doi.org/10.1111/j.1365-246X.2012.05432.x>
- Liang, C., Agram, P., Simons, M., & Fielding, E. J. (2019). Ionospheric Correction of InSAR Time Series Analysis of C-band Sentinel-1 TOPS Data. *IEEE Transactions on Geoscience and Remote Sensing*, *57*(9), 6755–6773. doi:[10.1109/TGRS.2019.2908494](https://doi.org/10.1109/TGRS.2019.2908494)
- Mears, C. A., Wang, J., Smith, D., & Wentz, F. J. (2015). Intercomparison of total precipitable water measurements made by satellite-borne microwave radiometers and ground-based GPS instruments. *Journal of Geophysical Research: Atmospheres*, *120*(6), 2492–2504. doi:<https://doi.org/10.1002/2014JD022694>
- Morishita, Y., Lazecky, M., Wright, T. J., Weiss, J. R., Elliott, J. R., & Hooper, A. (2020). LICSBAS: An Open-Source InSAR Time Series Analysis Package Integrated with the LiCSAR Automated Sentinel-1 InSAR Processor. *Remote Sensing*, *12*(3), 424.
- Nijholt, N., Simons, W. J. F., Efendi, J., Sarsito, D. A., & Riva, R. E. M. (2021). A Transient in Surface Motions Dominated by Deep Afterslip Subsequent to a Shallow Supershear Earthquake: The 2018 Mw7.5 Palu Case. *Geochemistry, Geophysics, Geosystems*, *22*(4), e2020GC009491. doi:<https://doi.org/10.1029/2020GC009491>
- Panuntun, H. (2021). Geodetic slip model of the November 26, 2019 Albania earthquake estimated from Sentinel-1 TOPS interferometry. *Tectonophysics*, *807*, 228814. doi:<https://doi.org/10.1016/j.tecto.2021.228814>
- Panuntun, H., Miyazaki, S., Fukuda, Y., & Orihara, Y. (2018). Probing the Poisson's ratio of poroelastic rebound following the 2011 Mw 9.0 Tohoku earthquake. *Geophysical Journal International*, *215*(3), 2206–2221. doi:[10.1093/gji/ggy403](https://doi.org/10.1093/gji/ggy403)
- Pepe, S., De Siena, L., Barone, A., Castaldo, R., D'Auria, L., Manzo, M., Casu, F., Fedi, M., Lanari, R., Bianco, F., & Tizzani, P. (2019). Volcanic structures investigation through SAR and seismic interferometric methods: The 2011–2013 Campi Flegrei unrest episode. *Remote Sensing of Environment*, *234*, 111440. doi:<https://doi.org/10.1016/j.rse.2019.111440>
- Pratama, C., Meilano, I., Sunarti, E., Haksama, S., & Sulistiyo, M. D. (2020, 24–26 June 2020). *Data-Driven of Time Series Decomposition on Estimating Geodetic Secular Motion Around Palu- Koro Fault Zone*. Paper presented at the 2020 8th International Conference on Information and Communication Technology (ICOICT).
- Qiu, J., Ji, L., Liu, L., & Liu, C. (2019). Seismogenic fault and tectonic significance of 1996 Karakoram Pass earthquake (Ms 7.1) based on InSAR. *Earth, Planets and Space*, *71*(1), 108. doi:[10.1186/s40623-019-1089-4](https://doi.org/10.1186/s40623-019-1089-4)
- Socquet, A., Hollingsworth, J., Pathier, E., & Bouchon, M. (2019). Evidence of supershear during the 2018 magnitude 7.5 Palu earthquake from space geodesy. *Nature Geoscience*, *12*(3), 192–199. doi:[10.1038/s41561-018-0296-0](https://doi.org/10.1038/s41561-018-0296-0)
- Song, X., Zhang, Y., Shan, X., Liu, Y., Gong, W., & Qu, C. (2019). Geodetic Observations of the 2018 Mw 7.5 Sulawesi Earthquake and Its Implications for the Kinematics of the Palu Fault. *Geophysical Research Letters*, *46*(8), 4212–4220. doi:<https://doi.org/10.1029/2019GL082045>
- Tobita, M. (2016). Combined logarithmic and exponential function model for fitting postseismic GNSS time series after 2011 Tohoku-Oki earthquake. *Earth, Planets and Space*, *68*(1), 41. doi:<https://doi.org/10.1186/s40623-016-0422-4>
- USGS. (2018). Earthquake Catalog Released by U.S Geological Survey. Retrieved from <https://earthquake.usgs.gov/earthquakes/eventpage/us1000h3p4/executive>

- Watson, A. R., Elliott, J. R., & Walters, R. J. (2022). Interseismic Strain Accumulation Across the Main Recent Fault, SW Iran, From Sentinel-1 InSAR Observations. *Journal of Geophysical Research: Solid Earth*, *127*(2), e2021JB022674. doi:<https://doi.org/10.1029/2021JB022674>
- Yu, C., Li, Z., Penna, N. T., & Crippa, P. (2018). Generic Atmospheric Correction Model for Interferometric Synthetic Aperture Radar Observations. *Journal of Geophysical Research: Solid Earth*, *123*(10), 9202-9222. doi:<https://doi.org/10.1029/2017JB015305>
- Yu, C., Penna, N. T., & Li, Z. (2017). Generation of real-time mode high-resolution water vapor fields from GPS observations. *Journal of Geophysical Research: Atmospheres*, *122*(3), 2008-2025. doi:<https://doi.org/10.1002/2016JD025753>